# **11A.4** EVOLUTION OF UPPER TROPOSPHERIC ZONAL MOMENTUM OVER THE WESTERN INDIAN OCEAN PRECEDING MADDEN-JULIAN OSCILLATION DEEP CONVECTIVE ONSET

Jennifer A. Gahtan* and Paul E. Roundy
University at Albany- State University of New York, Albany, New York

## 1. INTRODUCTION

While circulation signals associated with the Madden-Julian Oscillation circumnavigate through the tropics, MJO deep convection is confined to the warm pool region and often initiates over the western Indian Ocean. For MJO deep convection to develop, observational studies of the MJO (Powell and Houze 2013, 2015) and for convection in general (Hohenegger and Stevens 2012) suggest that the large-scale dynamics must be favorable to allow for upward motion. Circulation signals that often precede the onset of MJO deep convection include upper tropospheric easterly winds that circumnavigate the Western Hemisphere (e.g. Straub 2013). Furthermore, over the eastern Pacific Ocean, those easterly winds do not propagate eastwards through Kelvin wave type dynamics, but are instead advected by extratropical wavetrains and equatorial Rossby waves (Sakaeda and Roundy 2015a, b). To better understand the nature of the easterlies as they reach the western Indian Ocean, the work herein calculates a zonal momentum budget and uses a regional index to select events.

## 2. DATA AND METHODS

### a. Data

Outgoing longwave radiation (OLR) data from NOAA are used as a proxy for convection (Liebmann and Smith 1996). ECMWF Reanalysis Interim data are used for winds and geopotential height (Dee et al. 2011). Anomalies from climatology are calculated by removing the seasonal cycle and its first two harmonics. Intraseasonal anomalies are obtained by using a Lanczos Filter for 20-100 days with 201 weights (Duchon 1979).

### b. Time extended EOF

As analysis is focused on a regional scale, and global indices struggle to resolve signals near eastern Africa and the western Indian Ocean, we create a regional index based on the temporal evolution of the meridional structure in OLR between 20-70°E. Practically, this involves a calculation for a time-extended meridional EOF spanning 25 days before to 25 days after every day and 40 degrees south of to 40 degrees north of a selected seasonal cycle centered latitude.

The leading two EOFs explain around 11% of the variance apiece, while the EOFs and PCs are shifted 90° out of phase with one another and thus represent a propagating pattern. The resulting structure of the EOF shows OLR anomalies that begin in the subtropics then shift equatorwards about 10 days later. Using a method similar to Wheeler and Hendon (2004), an index of phases and amplitudes is created from the phase space of the PCs against one another, and the PCs are rotated for convenience to best match the RMM index.

Phase 1 events for the Intraseasonal Meridional Mode Index (IMMI) are selected for the months of November through May from November 1979- March 2012, when negative OLR begins to form over the western Indian Ocean. All events chosen have an amplitude greater than one, and only one event is chosen based on the phase angle of the event in each span of 10 days, to better find events in the same stage of development.

### c. Zonal momentum budget

The zonal momentum budget is given by:

$$u_t = -\mathbf{v} \cdot \boldsymbol{\nabla} u - \phi_x + fv + X, \quad (1)$$

where $\mathbf{v}$ contains the zonal, meridional, and vertical winds; subscripts represent partial derivatives; $\boldsymbol{\nabla}$ is the three dimensional gradient operator; $\phi$ is the geopotential height; f is the Coriolis parameter; and *X*, the residual, is taken as the difference between the time tendency and sum of the other terms. All terms herein are calculated at the 200hPa surface and filtered for intraseasonal timescales of 20-100 days.

## 3. RESULTS

*Corresponding author address: Jennifer A. Gahtan, SUNY-Albany DAES, Albany, NY, 12222;
email: jgahtan@albany.edu

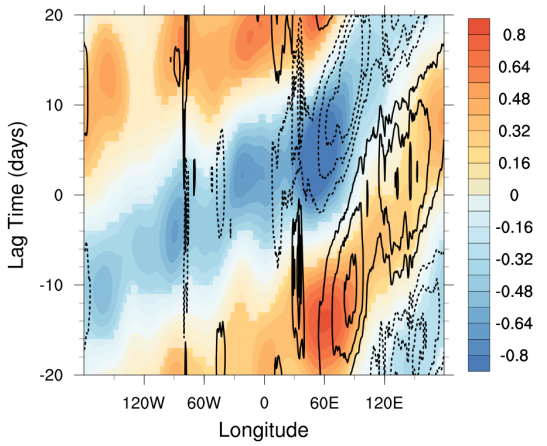


**Figure 1**: Lag time versus longitude diagram of the intraseasonal time tendency of zonal momentum ($10^{-5}$ $ms^{-2}$) 200hPa in shading and intraseasonal vertical velocity at 500hPa in contours averaged from 10°S-10°N for IMMI composites. Contours are from -0.015 to 0.015 hPa $s^{-1}$ with step sizes of 0.005 hPa $s^{-1}$, no contours at 0, and upward vertical motion shown by the dashed line.

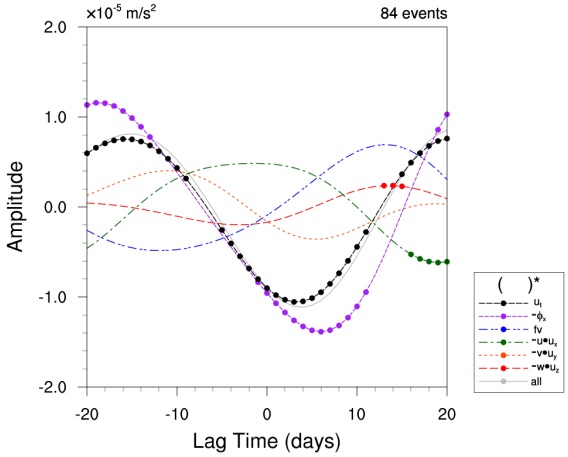


**Figure 2**: Full intraseasonal terms within the zonal momentum budget at 200hPa averaged between 10°S-10°N and 40-70°E for IMMI. Markers represent where values are significant. All represents the addition of all terms other than the tendency term.

Easterly acceleration circumnavigates across the Atlantic Ocean, reaching the western Indian Ocean around lag zero (Figure 1, shading) and maximizing in strength around 40-70°E. Upward motion at 500hPa (Figure1, contours) and 200hPa divergence (not shown) are also in phase over the Indian Ocean. A physical relationship between these fields suggests that easterly acceleration intruding on the western side of a region of westerlies leads to a flow pattern of divergence that may help to induce upward motion.

As the easterly acceleration peaks in amplitude near 40-70°E and 10°S-10°N at lag zero, we calculate the box averaged terms for the region over lag time. In the box, the time tendency reaches its minimum 3 days after lag zero (Figure 2, black line). The term that best phases with the time tendency and provides the largest quantity of easterly acceleration at lag zero is the pressure gradient force (PGF) (Figure 2, purple line).

Since the PGF term contributes the most easterly acceleration in the box at lag zero for the composite, we further focus on only the events that provide easterly acceleration from the PGF at lag zero. These events consist of 62 out of the 84 selected events and are thus a majority of the total cases.

While the importance of the PGF could indicate the presence of Kelvin wave type dynamics, unlike the overall tendency (Figure 3, contours) the easterly PGF signal does not circumnavigate in the tropics (Figure 3, shading).

Rather, negative PGF moves from the extratropics to the tropics between 40-70°E from both hemispheres, though stronger for the Northern Hemisphere (Figure 4, shading). This result is consistent with a reduction in positive geopotential height anomalies that may result from a wavetrain that intrudes into the tropics along the East coast of Africa (Figure 4, contours). Similarly, the intraseasonal streamfunction anomalies allow for equatorward flow over Africa, which concurs with incoming wavetrains over the region (not shown).

## 4. DISCUSSION

The circumnavigating easterly acceleration may help to provide a dynamical forcing necessary for the formation of MJO deep convection, because as it encroaches on the west side of a region of intraseasonal westerlies, a flow pattern of upper level divergence forms.

For a majority of the cases, easterly acceleration is due a positive pressure gradient that forms between the east coast of Africa and the western Indian Ocean. Instead of circumnavigating, which would suggest Kelvin wave type dynamics, negative geopotential height anomalies move from the extratropics to the tropics near the east coast of Africa, forcing the easterly acceleration and potentially helping with the onset of MJO deep convection.

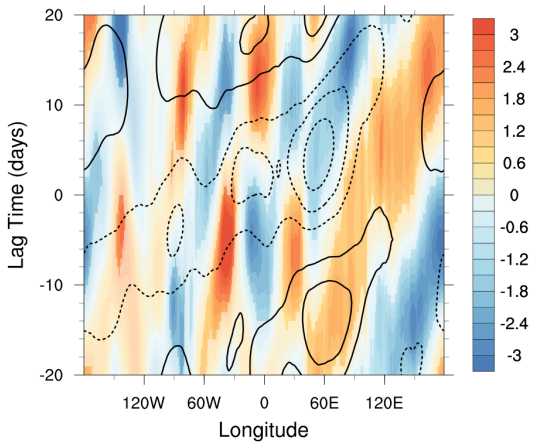


Figure 3: Intraseasonal pressure gradient force ($10^{-5}$ms$^{-2}$, shading) and time tendency ($10^{-5}$ms$^{-2}$, contours) for IMMI events averaged 10°S-10°N.

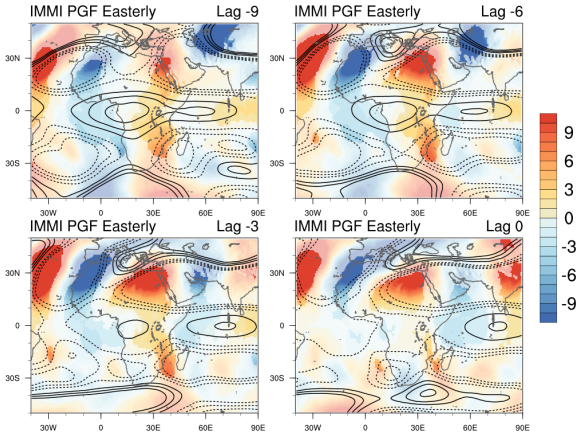


Figure 4: Intraseasonal pressure gradient force ($10^{-5}$ms$^{-2}$, shading) and geopotential height (contours) for IMMI events where the PGF is easterly at lag zero from 10°S-10°N and 40-70°E, at lags of -9, -6, -3, and 0 days.

## 5. REFERENCES


Dee, D. P., and Coauthors, 2011: The ERA-Interim reanalysis: Configuration and performance of the data assimilation system. *Q. J. R. Meteorol. Soc.*, **137**, 553–597, https://doi.org/10.1002/qj.828.

Duchon, C., 1979: Lanczos Filtering in One and Two Dimensions. *J. Appl. Meteorol.*, https://doi.org/10.1175/1520-0450(1979)018<1016:LFIOAT>2.0.CO;2.

Hohenegger, C., and B. Stevens, 2012: Preconditioning deep convection with cumulus congestus. *J. Atmos. Sci.*, 120821112333009, https://doi.org/10.1175/JAS-D-12-089.1.

Liebmann, B., and C. a. Smith, 1996: Description of a complete (interpolated) outgoing longwave radiation datasets. *Bull. Amer. Meteor. Soc.*, **77**, 1275–1277.

Powell, S. W., and R. A. Houze, 2013: The cloud population and onset of the Madden-Julian Oscillation over the Indian Ocean during DYNAMO-AMIE. *J. Geophys. Res. Atmos.*, **118**,11,979-11,995, https://doi.org/10.1002/2013JD020421.

——, and ——, 2015: Effect of dry large-scale vertical motions on initial MJO convective onset. *J. Geophys. Res. Atmos.*, **120**, 4783–4805, https://doi.org/10.1002/2014JD022961.

Sakaeda, N., and P. E. Roundy, 2015a: The Development of Upper-Tropospheric geopotential height anomaly in the Western Hemisphere during MJO convective initiations. *Q. J. R. Meteorol. Soc.*, **142**, https://doi.org/10.1002/qj.2696.

——, and P. E. Roundy, 2015b: The Development of Upper-Tropospheric Wind over the Western Hemisphere in Association with MJO Convective Initiation. *J. Atmos. Sci.*, **72**, 3138–3160, https://doi.org/10.1175/JAS-D-14-0293.1.

Straub, K. H., 2013: MJO initiation in the real-time multivariate MJO index. *J. Clim.*, **26**, 1130–1151, https://doi.org/10.1175/JCLI-D-12-00074.1.

Wheeler, M. C., and H. H. Hendon, 2004: An All-Season Real-Time Multivariate MJO Index: Development of an Index for Monitoring and Prediction. *Mon. Weather Rev.*, **132**, 1917–1932, https://doi.org/10.1175/1520-0493(2004)132<1917:AARMMI>2.0.CO;2.

2017: The NCAR Command Language. https://doi.org/10.5065/D6WD3XH5.